Journal of Photochemistry and Photobiology A: Chemistry 217 (2011) 22–28

Contents lists available at ScienceDirect

Journal of Photochemistry and Photobiology A: Chemistry

journal homepage: www.elsevier.com/locate/jphotochem

Development and characterization of a titanosilicate ETS-10-coated optical fiber reactor towards the photodegradation of methylene blue

Zhaoxia Ji, Dennis M. Callahan Jr., Mariam N. Ismail, Juliusz Warzywoda, Albert Sacco Jr.*

Center for Advanced Microgravity Materials Processing, Department of Chemical Engineering, Northeastern University, Boston, MA 02115, USA

ARTICLE INFO

Article history:
Received 1 March 2010
Received in revised form 7 September 2010
Accepted 16 September 2010
Available online 22 September 2010

Keywords:
ETS-10
Methylene blue
Optical fiber reactor
Photocatalysis
Quantum efficiency
Titanosilicates

ABSTRACT

An optical fiber reactor (OFR) system containing uniformly distributed quartz fibers coated with titanosilicate ETS-10 crystals was investigated. Optimum ETS-10 film thickness (~1.5 μm) and coating length (15 cm) were determined from the light propagation analysis in a single ETS-10-coated fiber. The nearly constant value of the attenuation coefficient ($\alpha \approx 0.10\,cm^{-1}$) for films with different thickness indicated uniform fiber surface coverage with these films. The extinction coefficient, ε, decreased from ~1.6 to ~1.0 μm^{-1} with ETS-10 film thickness increasing from ~0.5 to ~1.5 μm, which suggested less contact per unit film thickness between light and ETS-10 crystals inside thicker films, likely due to their lower crystal packing density. Photodegradation of methylene blue (MB) conducted in the OFR showed higher photocatalytic activity for thicker ETS-10 films. Although higher MB photodegradation rates were obtained at higher light intensity, the apparent quantum efficiency, Φ, decreased with increasing light intensity. This is consistent with the charge separation mechanism for MB photodegradation in the UV light range investigated. All ETS-10 samples investigated showed ~4–5 times higher Φ values in the OFR than in the slurry reactor, likely due to the unique light/photocatalyst/reactant contact and high fiber packing density in the OFR.

1. Introduction

Titanosilicate ETS-10 is a crystalline open-framework material built of corner-sharing TiO_6 octahedra and SiO_4 tetrahedra [1]. The uniform micropores (pore size 4.9 Å × 7.6 Å) together with non-framework cations (Na^+ and K^+ in the as-synthesized crystals) that balance the net negative charge of the framework, give ETS-10 catalytic, ion exchange, adsorption, and molecular separation properties [2]. The framework of ETS-10 contains monatomic linear semiconducting . . .Ti–O–Ti–O–Ti. . . chains that are effectively separated from each other by the silica matrix [3]; and are regarded as a quantum-confined form of titania (TiO_2) with a bandgap energy of ~4.03 eV [4]. ETS-10 is a promising photocatalyst/semiconductor in such applications as photodegradation of organic chemicals [5–8], water splitting [9], and solar cells [10]. The photocatalytic activity of ETS-10 can be modified/improved by Ag ion exchange [6] and transition metal isomorphous substitution [6,7]. Previous investigations using as-synthesized or modified ETS-10 crystals in liquid phase photocatalysis were performed in slurry reactors [5,8,9]. However, slurry reactors are not suited for practical applications because they require additional separation and recycling process, which can be inconvenient, time-consuming, and expensive [11]. Recently, more attention has been paid to immobilized photocatalytic reactor systems, particularly the optical fiber reactor (OFR) system in which optical fibers are used as both a light transmission tool and a photocatalyst support. This design allows the light to directly reach the photocatalyst coated on the optical fiber surface without passing through the liquid; thus, reduces the light loss due to liquid absorption. The small diameter of optical fibers and high fiber packing density in the OFR system also provide high illuminated photocatalyst surface area within a reactor volume compared to the conventional immobilized reactor system. It is expected that the mass transfer limitations can be also reduced/eliminated in this type of distributive configuration as the penetration distance for the light to reach the catalyst and the average distance for reactant diffusion to the photocatalyst surface decreases in comparison with that in a conventional immersion type reactor, where a single lamp is usually used for illumination. A practical OFR system for photocatalysis was first developed by Hofstadler et al. [12], and further investigated/improved by Peill and Hoffmann [13,14]. Although increasing attention has been paid to this type of system for photocatalysis in both liquid and gas phases, all OFR systems have been designed based on TiO_2-coated optical fibers [12–18]. A drawback of TiO_2-based OFR systems is the

* Corresponding author. Tel.: +1 617 373 7912; fax: +1 617 373 2209.
E-mail address: asacco@coe.neu.edu (A. Sacco Jr.).

1010-6030/$ – see front matter © 2010 Elsevier B.V. All rights reserved.
doi:10.1016/j.jphotochem.2010.09.011

short (less than 10 cm [13,19]) maximum light propagation distance of UV light along the coated optical fibers. This is mainly due to the high refractive index incompatibility between TiO_2 and quartz optical fibers in the UV light range (i.e., ~2.4–2.6 for TiO_2 vs. ~1.4–1.5 for quartz [12,13,15]). Increased light propagation along the fibers enhances the activated photocatalytic surface area, thus resulting in increased quantum efficiency in an OFR system [13]. The anticipated lower refractive index of ETS-10 (roughly estimated to be similar to those for aluminum silicates, i.e., ~1.7–1.9 [20]) compared to TiO_2 is expected to result in slower refraction loss, thus more uniform light distribution along the ETS-10-coated optical fibers, and consequently higher light use efficiency. In this paper, an OFR system containing uniformly distributed ETS-10-coated optical quartz fibers was designed. Light distribution in a single ETS-10-coated optical fiber was characterized, and the effects of film thickness and coating length were investigated. To improve the photocatalytic activity of as-synthesized Na^+, K^+-ETS-10 (unmodified ETS-10), cobalt isomorphously substituted ETS-10 (Co-ETS-10) and silver ion-exchanged ETS-10 (Ag^+-ETS-10) were also prepared. The photocatalytic activities of unmodified ETS-10, Co-ETS-10, and Ag^+-ETS-10 in degradation of methylene blue (MB) dye in the developed OFR system were determined. The apparent quantum efficiencies for MB photodegradation on these samples were compared for the OFR and the slurry reactor.

2. Materials and methods

2.1. ETS-10 crystals and thin film preparation

The unmodified ETS-10 crystals and Co-ETS-10 crystals for use in the slurry reactor (i.e., as powder) were hydrothermally synthesized according to the literature procedures [21] and [6], respectively. The unmodified ETS-10 and Co-ETS-10 thin films for use in the OFR were obtained by dip coating the fiber bundle assembly (i.e., optical fibers and aluminum plates) in an ethanol (200 proof) suspension containing 5 wt.% of the unmodified ETS-10 and Co-ETS-10 crystals, respectively, followed by drying in ambient air at ~523 K for 10 min. Once the coated fiber bundle assembly was prepared, it was gently slid into the reactor vessel. The crystals loosely attached on the fiber surface as well as on the aluminum plates were removed by pumping 1 L of deionized water through the reactor for 30 min. The Ag^+-ETS-10 thin films for use in the OFR were obtained by pumping 200 mL of aqueous $AgNO_3$ solution through the reactor with the unmodified ETS-10 films for 2 h at 293 K. The mass ratio of unmodified ETS-10 crystals to dissolved $AgNO_3$ was kept at 2:1. After Ag ion exchange, 1 L of deionized water was circulated through the reactor for 10 min to remove the excess Ag^+ ions as well as NO_3^- ions. For use in a slurry reactor, the Ag^+-ETS-10 samples were prepared by stirring 200 mL aqueous suspensions containing the unmodified ETS-10 crystals and dissolved $AgNO_3$ crystals in a 2:1 mass ratio for 2 h at ~353 K to achieve the Ag ion exchange level similar to that obtained in the OFR. After ion exchange, the samples were filtered and washed with 1 L of deionized water, followed by overnight drying at 353 K in ambient air.

2.2. Characterization techniques

X-ray powder diffraction (XRD, Bruker D5005 θ:2θ diffractometer, CuKα radiation, 40 kV, 30 mA) was used to verify the identity of ETS-10 crystals synthesized, incorporation of Co into the ETS-10 framework, and Ag ion exchange in ETS-10 crystals. Field emission scanning electron microscopy (FE-SEM, Hitachi S-4700 FE-SEM, secondary electron imaging mode, accelerating voltage 2 kV, beam current 10 μA, working distance 3 mm) was used to image the morphology of ETS-10 crystals and coverage of optical fibers with crystals, and determine the thickness of ETS-10 films deposited on optical fibers. Energy dispersive X-ray spectroscopy (EDX, Phoenix EDAX X-ray analyzer equipped with a Sapphire super ultra thin window detector attached to the Hitachi S-4700 FE-SEM, accelerating voltage 20 kV, beam current 10 μA, working distance 12 mm, counting time 100 s) was used to determine the relative silver (Ag/Ti) and cobalt (Co/Ti) concentration in Ag^+-ETS-10 and Co-ETS-10 crystals, respectively; and to determine the crystal Si/Ti ratio in the unmodified and modified ETS-10 samples. Diffuse reflectance (DR) UV–vis spectroscopy (Cary 5000 UV–vis–NIR spectrometer equipped with a Praying Mantis accessory) was performed to obtain the optical and electronic properties of the unmodified and modified ETS-10 samples. Powdered Spectralon™ standard was used as reference. The measurements were conducted in ambient air using a bandwidth of 1.0 nm.

2.3. Light intensity measurements in a single optical fiber

For the single fiber light transmission and distribution analysis, light intensities for the individual unstripped optical fibers as well as ETS-10-coated and uncoated (bare) fibers after buffer coating/cladding removal were measured using a UVX radiometer equipped with a UVX-31 sensor. Light intensities were measured at the end of the ETS-10-coated fiber and on the outer surface of ETS-10 thin film at different axial lengths. The light intensity at the end of an unstripped optical fiber was taken as the incident light intensity. The light source used and the method of light filtering/focusing are described in Section 2.4.

2.4. Optical fiber reactor system setup

The OFR system consisted of a custom-built reactor vessel, an ETS-10 crystals-coated fiber bundle, a light source, and a peristaltic pump. The liquid was pumped through the reactor and recycled back into the reactor via silicone tubing. The reactor vessel was made of an acrylic cylinder (diameter = 4.13 cm), and contained an aluminum base plate and five perforated aluminum plates utilized to hold and distribute optical fibers inside the reactor. Each perforated plate had 100 holes (hole diameter = 1.5 mm) concentrically arranged at a spacing of 1.5 mm. Except for the top one, each plate had a cut edge to introduce cross flow in the reactor. When placed in the reactor, the five plates were connected and evenly separated at a 2.52 cm interval using aluminum pins. The total volume of this reactor was ~200 mL. The reactor vessel was set up vertically with the inlet located at the bottom and outlet at the top of the reactor (Fig. 1a). A fiber bundle containing 100 individual quartz optical fibers (Optran HUV1000/1035T, 1 mm core diameter) was prepared and polished at the bundled end by CeramOptec Industries. At the free end, all fibers were stripped of buffer coating. The stripped part was treated for ~10 min at ~393 K in a 98% sulfuric acid to remove the cladding. The exposed fiber core was ultrasonicated for 30 min and thoroughly rinsed in deionized water, and dried at 343 K in ambient air. Light was supplied by a 500 W Xe arc lamp (Oriel Model 66924). A dichroic mirror (280–400 nm), followed by a UVB/C blocking filter (310–400 nm) when required, was used to deliver UV light. The filtered light was then focused into the optical fiber bundle using a plano-convex lens (250 mm focal length) to obtain an incident angle of 84.2° (Fig. 1b).

2.5. Photocatalytic tests in the optical fiber reactor and the slurry reactor

All photocatalytic experiments were performed at room temperature (298 ± 3 K). The optimum ETS-10 film thickness and fiber coating length used in the OFR system were determined based on

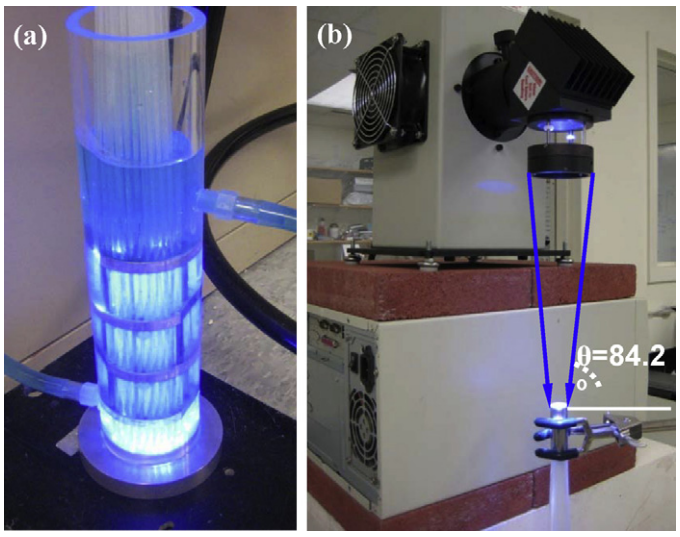

Fig. 1. The optical fiber reactor system containing (a) a cylindrical reactor vessel, and (b) a UV light source with an incident angle of 84.2°.

the results of light distribution analysis in a single-ETS-10-coated fiber (Sections 3.3 and 3.4). For degradation of MB in the OFR, the reactor was fed with ~200 mL aqueous MB solution (concentration = 10 mg L^{-1}, pH = 5.4), and circulated for 1 h in the dark before irradiating with UV light to achieve adsorption/desorption equilibrium. To obtain different light intensities, the distance between the fiber bundle front tip and the lamp was adjusted. To investigate the external mass transfer effect on MB photodegradation on unmodified ETS-10 in the OFR, the flow rate was increased from 0.8 to 4.0 L min^{-1}. A constant value for the reaction rate constant, which suggested the elimination of external mass transfer limitations, was obtained at flow rates higher than 3.0 L min^{-1}. Therefore, all experiments were performed using flow rate of 3.5 L min^{-1} to ensure the kinetic control in the OFR. Experiments in the slurry reactor were carried out in a 400 mL Pyrex beaker using crystals (concentration = 500 mg L^{-1}) suspended in 200 mL aqueous MB solution (concentration = 10 mg L^{-1}, pH = 5.4). Prior to irradiation with UV light, the suspension was stirred in the dark for 1 h to achieve adsorption/desorption equilibrium. The distance between the top surface of reaction mixture and the lamp was fixed at 10 cm. To investigate the external mass transfer effect on MB photodegradation in the slurry reactor on unmodified ETS-10, the stirring rate was increased from 500 to 1000 rpm. With rates higher than 750 rpm, the reaction rate constant was independent on stirring rate, indicative of no external mass transfer limitations. Therefore, the stirring rate of 1000 rpm was used to ensure the kinetic control in the slurry reactor. The pH of 5.4 used in all photocatalytic experiments was determined based on the MB photodegradation results obtained from the slurry reactor, which showed that in the pH range 2.5–9.2 (pH was adjusted by adding 0.1 M aqueous NaOH solution or 0.1 M aqueous HCl solution to the ETS-10 suspension) the highest photocatalytic activity of unmodified ETS-10 was obtained at pH of 4.0–5.4. Without light irradiation, no degradation of MB was observed. Extremely slow degradation of MB carried out in the slurry reactor under UV light irradiation in the absence of ETS-10 (reaction rate constant ≈ 0.005 min^{-1}) suggested the contribution of direct UV light MB photolysis to degradation of MB on the ETS-10 samples is insignificant under conditions used in this investigation. The degradation of MB was monitored using a Cary 5000 UV–vis–NIR spectrometer. The concentration of MB was determined from the intensity of the absorbance maximum at the wavelength of ~664 nm due to MB in the UV–vis spectrum [22].

3. Results and discussion

3.1. ETS-10 crystals and films

The unmodified ETS-10 product was highly crystalline and phase-pure, as determined by XRD analysis (Fig. 2a). This material gave a bandgap energy (E_g) of ~4.00 eV, as determined from its UV–vis spectrum (Fig. 2b) using the method described in the literature [7]. Successful isomorphous substitution of Co for Si in the highly crystalline and phase-pure Co-ETS-10 product was ascertained by the slight shift of the XRD peaks to lower angels (Fig. 2a), a slight shift in the bandgap to lower energy ($E_g \approx 3.82$ eV), and the observation of the 500–600 nm absorption band in its UV–vis spectrum (Fig. 2b), as previously reported [23]. EDX analysis showed the crystal Co/Ti ratio of 0.055. Successful Ag ion exchange in the Ag^+-ETS-10 crystals was determined from the red shift in the absorption edge ($E_g \approx 3.62$ eV) compared to that of the parent unmodified ETS-10 crystals (Fig. 2b). XRD analysis revealed the intensities of 200, 204 (Fig. 2a), and 224 reflections increased, whereas the intensities of remaining peaks decreased in Ag^+-ETS-10 compared to unmodified ETS-10. This also indicated Ag ion exchange in Ag^+-ETS-10 [24]. Similar decrease in peak intensities was observed in Rb^+- and Cs^+-exchanged ETS-10 by Goa et al. [25], who attributed this to X-ray scattering from the exchanged cations instead of crystallinity loss. Thus, a similar conclusion may be drawn here for the Ag^+-ETS-10 samples. EDX analysis showed identical within experimental error Ag/Ti ratios for the Ag^+-ETS-10 powder (1.28 ± 0.13)

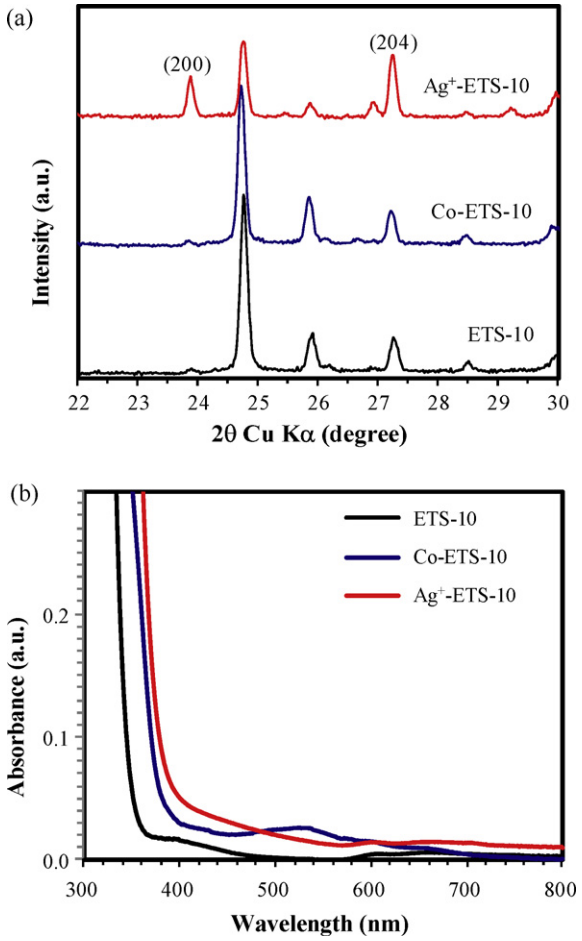

Fig. 2. (a) XRD patterns of the unmodified ETS-10 (ETS-10), Co-ETS-10, and Ag^+-ETS-10 samples; (b) UV–vis spectra of the unmodified ETS-10 (ETS-10), Co-ETS-10, and Ag^+-ETS-10 samples.

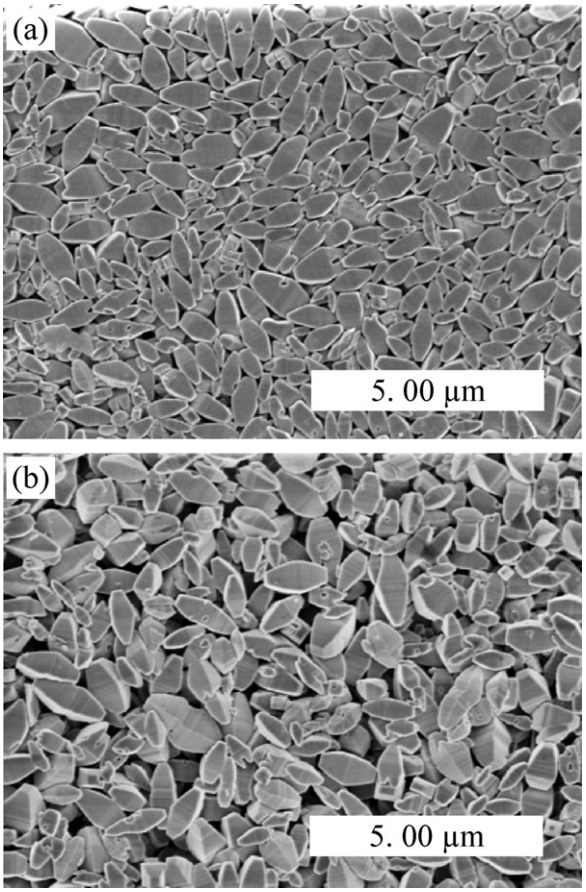

Fig. 3. FE-SEM images of ETS-10 films prepared on optical fibers using: (a) single dip coating, and (b) triple dip coating.

and the Ag^+-ETS-10 film (1.10 ± 0.11). This allowed the unambiguous comparison of the results for photocatalytic degradation of MB on Ag^+-ETS-10 in the OFR and the slurry reactor. FE-SEM analysis suggested that both the cobalt substitution and silver ion exchange did not alter size, morphology, or surface features of ETS-10 crystals (images not shown).

One, two, and three dip coating steps resulted in ETS-10 films with the thickness of ~0.5, ~1.0, and ~1.5 μm, respectively, as determined by FE-SEM analysis of film cross-sections. A single dip coating resulted in a nearly continuous film composed of a monolayer of ETS-10 crystals. FE-SEM analysis indicated a considerable *a*(*b*)-out-of-plane preferred orientation of ETS-10 crystals in the monolayer thin film prepared from single dip coating (Fig. 3a). Crystals in multilayer films obtained using two and three dip coating steps were less preferentially oriented (Fig. 3b). The multilayer films showed larger gaps between crystals on the outer film surface (i.e., lower crystal packing density) compared to the monolayer film (Fig. 3).

3.2. Development of light transmission model in a single optical fiber

In an ETS-10-coated fiber, the light flux is divided into two parts: one part is reflected inside the optical fiber, and the other is refracted into the ETS-10 film, part of which is subsequently absorbed by ETS-10 crystals for photocatalysis. The reflected part is transmitted along the fiber with light intensity loss after each contact with the ETS-10/optical fiber interface. The intensity of reflected light, I_l (mW cm^{-2}), at a distance l (cm) from the front tip of an ETS-10-coated optical fiber can be fitted with an exponential correlation based on Beer's law as:

$$I_l = I_{input}\, e^{-\alpha l} \tag{1}$$

where α is the attenuation coefficient of ETS-10 coating (cm^{-1}), and I_{input} is the incident light intensity (mW cm^{-2}). The intensity of the light refracted into ETS-10 film also exponentially decays upon light passing through the film. The light that is not absorbed by ETS-10 will be transmitted to the outer surface of the film, and its intensity on the outer surface of the film deposited on the fiber can be described as:

$$I_{l,\delta} = I_{refr}\, e^{-\varepsilon\delta} \tag{2}$$

where ε is the extinction coefficient of ETS-10 coating (μm^{-1}), δ is the coating thickness (μm), $I_{l,\delta}$ is the light intensity on the outer surface of the ETS-10 thin film with a thickness δ at a distance l from the optical fiber front tip (mW cm^{-2}), and I_{refr} is the intensity of the refracted light at the optical fiber/ETS-10 film interface at a distance l from the optical fiber front tip (mW cm^{-2}).

Assuming light loss other than refraction can be neglected and there is no light accumulation in the optical fiber with diameter D (cm), an energy shell balance of the light over a segment of dl will give the following correlation:

$$I_{ref} = \frac{D}{4} I_{input} \left(-\frac{de^{-\alpha l}}{dl} \right) \tag{3}$$

Thus, the refracted light intensity on the cylindrical surface of the optical fiber at a distance l from the front tip can be expressed as:

$$I_{refr} = \frac{D\alpha}{4} I_{input}\, e^{-\alpha l} \tag{4}$$

Substituting Eq. (4) into Eq. (2) will give the intensity of the light on the outer surface of the ETS-10 thin film with a thickness δ at a distance l from the front tip of the optical fiber with a diameter D as:

$$I_{l,\delta} = \frac{D\alpha}{4} I_{input}\, e^{-\varepsilon\delta}\, e^{-\alpha l} \tag{5}$$

In Eq. (5), both $I_{l,\delta}$ and I_{input} can be measured, and D is known; therefore, the attenuation coefficient, α, and the extinction coefficient, ε, for various coating lengths and thin film thicknesses can be determined.

3.3. Light transmission along a single ETS-10-coated fiber

Light transmission for a TiO_2-coated quartz optical fiber is similar in aqueous system and in air [15]. Therefore, single-ETS-10-coated-fiber light transmission analysis was performed in air for the ease of measurements. Thus determined optimum ETS-10 film thickness and coating length were used in the design of the OFR system for liquid phase photodegradation of MB. Fig. 4 shows the measured light intensity decay along the coated length in the optical fibers with coating thickness of ~1.5 μm, and different ETS-10 coating lengths of 10, 15, 20, and 30 cm. The data in Fig. 4 were fitted using Eq. (5) to determine the attenuation coefficient, α. The intensity measured at the end of each coated fiber was not included in the fitting to avoid the end effects [26]. The α values were determined to be 0.14 ± 0.02, 0.10 ± 0.02, 0.10 ± 0.02, and 0.08 ± 0.02 cm^{-1} for the optical fiber with ETS-10 coating length of 10, 15, 20, and 30 cm, respectively. The α value did not show strong dependence on the ETS-10 coating length, which suggested relatively uniform ETS-10 thin films were prepared in all cases. The slight decrease in α value for the longer ETS-10-coated optical fibers suggested that light decays relatively slower along the fibers with the longer coating length (Fig. 4). However, in all cases, more than

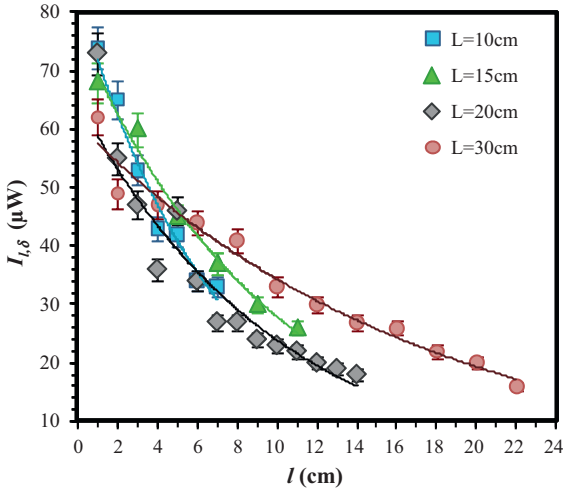

Fig. 4. Light intensity profiles along a single optical fiber with different coating length, *l*, determined on the outer surface of the unmodified ETS-10 films with thickness of ~1.5 μm.

80% of the incident light was lost within the first 15–20 cm. Therefore, optical fibers with a coating length of 15 cm were selected for photocatalytic investigation in the OFR system.

3.4. Light propagation through ETS-10 thin films

The activity of a photocatalyst film coated on optical fibers is related to the amount of the refracted light that is absorbed by the photocatalyst crystals in the film, which depends on the extinction coefficient, ε, of this film. The unmodified ETS-10 thin films with coating length of 15 cm, and different thicknesses of ~0.5, ~1.0, and ~1.5 μm, were prepared by increasing the number of dip coating steps (i.e., one, two, and three, respectively). The light propagation profiles along the fibers on the outer surface of these films are presented in Fig. 5. Although less light has remained on the outer surface of the thicker films, all three ETS-10 films showed similar attenuation coefficients ($\alpha \approx 0.10\,cm^{-1}$). Since the refraction loss is mainly determined by the properties of the interface between the optical fiber and photocatalyst film [13–15], the thickness-independence of α value suggested the uniform optical fiber surface coverage for all three ETS-10 films. The extinction coefficient, ε, was calculated from data in Fig. 5 using Eq. (5) to be ~1.6, ~1.3, and ~1.0 μm^{-1} for the ETS-10 films with thickness of ~0.5, ~1.0, and ~1.5 μm, respectively. Similar trend was reported for P25 TiO_2 coatings on a single quartz fiber [13]. The lower extinction coefficients; i.e., slower light decay for the thicker films (Fig. 5), suggested less contact per unit film thickness between light and the crystals inside the thicker films. This is likely due to the more loosely packed ETS-10 crystals in the multilayer films (Fig. 3). The higher intercrystal porosity could allow some of the light to propagate without being absorbed by ETS-10 crystals. Based on the ε values determined above, the fraction of the refracted light absorbed by ETS-10 crystals was estimated to be 55%, 72%, and 78% for the ETS-10 films with thickness of ~0.5, ~1.0, and ~1.5 μm, respectively. These results suggest that thicker ETS-10 films are preferred to achieve high light use efficiency. The light not absorbed by ETS-10 film was used to illuminate ETS-10 crystals coated on the aluminum plates in the OFR as described in Section 2.1.

3.5. Film thickness effect

The OFR system allows a unique light/photocatalyst/reactant contact where reactant diffuses into photocatalyst film from the "outer" surface of the film whereas light enters in the opposite direction from the "inner" surface of the film. Thus, it was hypothesized that an optimum thin film thickness is needed to achieve high light use efficiency; as a too thin film would result in the waste of light, whereas a too thick film would retard the diffusion of reactant throughout the film. To investigate the effect of ETS-10 film thickness, photocatalytic degradation of MB using ETS-10 films with thickness of ~0.5, ~1.0, and ~1.5 μm was conducted in the OFR system. Assuming the pseudo first-order reaction mechanism [22], the results showed increased photocatalytic activity of ETS-10 with the increased film thickness (Fig. 6). When the ~0.5 μm thick ETS-10 film was used, negligible conversion of MB was obtained. The reaction rate constant for the ~1.5 μm thick film was almost an order of magnitude higher than that for the ~1.0 μm thick film (Fig. 6). The increase in the number of dip coating steps above three did not result in thicker films, mostly likely due to the weak attachment of the crystals on the outer film surface. Therefore, the ~1.5 μm thick film prepared by triple dip coating was selected to investigate the light intensity effect as well as effects of Co isomorphous substitution or Ag ion exchange in ETS-10 crystals on photodegradation of MB on modified ETS-10 in the OFR system.

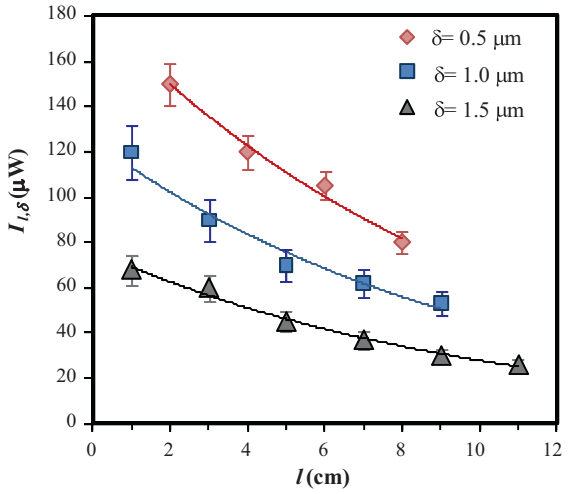

Fig. 5. Light intensity profiles along a single optical fiber with coating length of 15 cm determined on the outer surface of the unmodified ETS-10 films with different coating thickness, δ.

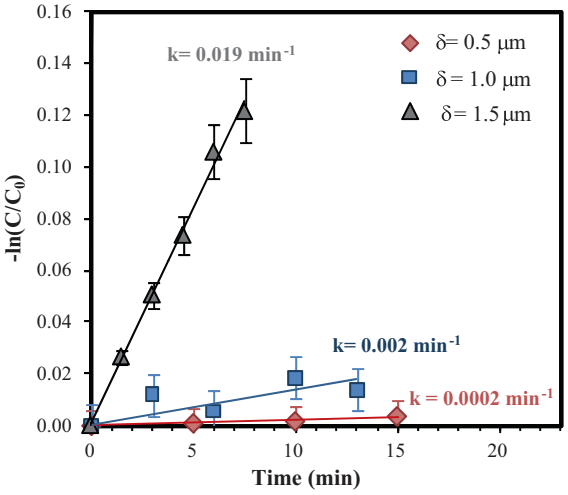

Fig. 6. Effect of the unmodified ETS-10 film thickness, δ, on the kinetics of photocatalytic degradation of methylene blue under 280–400 nm UV light irradiation with photon flux of 1.0×10^{17} photon s^{-1} in the OFR system.

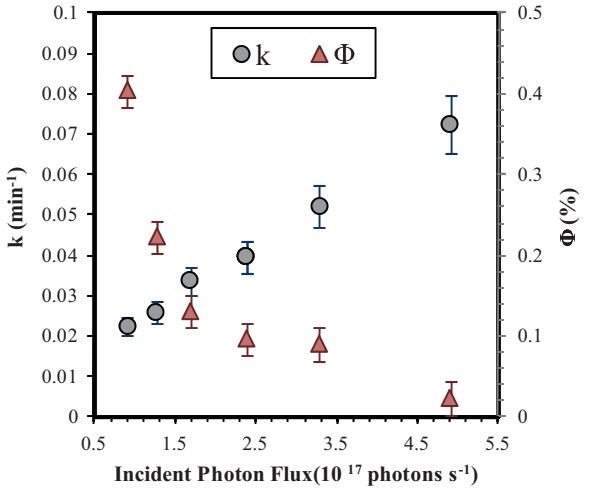

Fig. 7. Effect of incident photon flux on the reaction rate constant, *k*, and the apparent quantum efficiency, *Φ*, for the photodegradation of methylene blue on unmodified ETS-10 under 280–400 nm UV light irradiation in the OFR system.

3.6. Incident light intensity effect

The apparent quantum efficiency, *Φ*, defined as the number of reactant molecules converted per the number of photons supplied or the initial reaction rate divided by the incident photon flux measured at 365 nm [17,19], was calculated to evaluate the performance of the fabricated OFR:

$$\Phi = \frac{\text{reaction rate}}{\text{incident photon flux}} \approx \frac{N_A V_l dC_A/dt}{dN_{ph}/dt} \quad (6)$$

where N_A is the Avogadro's number (6.022×10^{23} molecules mol^{-1}), V_l is volume of the reaction solution (L), C_A is concentration of the reactant A (mol L^{-1}), t is reaction time (s), and N_{ph} is the number of photons supplied in time t.

The incident photon flux was varied from 6.05×10^{16} to 4.90×10^{17} photons s^{-1}. Although higher conversion of MB, and thus larger reaction rate constant was obtained at higher light intensity, i.e., higher incident photon flux, (Fig. 7), the apparent quantum efficiency, *Φ*, calculated using Eq. (6), decreased with increasing light intensity (Fig. 7). These results are similar to other literature data [14,16,17], which suggest that the rate of electron–hole recombination increases relative to the interfacial charge transfer rate at high light intensity. This agrees with the photocatalytic pathway for degradation of MB in the UV range investigated here [27], where the supraband gap photon-generated conduction band electrons and valence band holes from the ETS-10 semiconductor participate directly or indirectly via formation of reactive oxygen radicals (e.g., HO•, HO_2•) in the degradation of MB. The incident light intensity determines the rate of electron–hole pair generation, and consequently, the concentration of oxidative species that are responsible for the photodegradation of MB. At low light intensities, the photons supplied might not be sufficient to excite all of the active sites on the ETS-10 surface. An increase in the light intensity will lead to more electron–hole pair generation, along with the corresponding increase in oxidative species creation. However, when the light intensity reaches high levels, it also results in high electron–hole recombination. It has been reported that the electron–hole recombination and interfacial charge transfer are second- and first-order processes, respectively [28]. Therefore, the rate of electron–hole recombination increases faster than that of the interfacial charge transfer, resulting in lower quantum efficiency at high light intensity as shown in Fig. 7.

Table 1
Apparent quantum efficiency, *Φ*, of the unmodified ETS-10 (ETS-10), Co isomorphously substituted ETS-10 (Co-ETS-10), and Ag ion-exchanged ETS-10 (Ag^+-ETS-10) crystals in photodegradation of methylene blue under 310–400 nm UV light irradiation in the slurry reactor and the optical fiber reactor (OFR).

Sample *Φ*	Slurry reactor (%)	OFR (%)
ETS-10	0.03 ± 0.01	0.12 ± 0.01
Co-ETS-10	0.06 ± 0.01	0.33 ± 0.03
Ag^+-ETS-10	0.30 ± 0.03	1.42 ± 0.14

3.7. Efficiency comparison between optical fiber reactor and slurry reactor

Preliminary photocatalytic experiments in a slurry reactor showed that both Co-ETS-10 and Ag^+-ETS-10 had higher activity than unmodified ETS-10. Therefore, the performance of these modified samples was also evaluated in the designed OFR system. With both reactor systems operated in the kinetic-control regime, similar trends should be expected. Table 1 shows a comparison of the apparent quantum efficiency, *Φ*, for the unmodified ETS-10, Co-ETS-10, and Ag^+-ETS-10 samples used to photocatalytically degrade MB in the slurry reactor and the OFR. All ETS-10 samples showed approximately four- to five-fold apparent quantum efficiency improvement in the OFR compared to the slurry reactor (Table 1). The high activity achieved in the OFR system is most likely due to the high light use efficiency in such a system, where light directly reaches the photocatalyst coated on the optical fiber surface without passing through the liquid; and thus, the light loss due to liquid absorption is reduced. As shown in Table 1, Ag ion exchange and Co isomorphous substitution resulted in the enhancement of ETS-10 photocatalytic activity. This may be attributed to a somewhat broader UV irradiation range utilization by the modified ETS-10 samples compared to unmodified ETS-10, as indicated by the lower bandgap energy for Ag^+-ETS-10 (~3.62 eV) and Co-ETS-10 (~3.82 eV) than for unmodified ETS-10 (~4.00 eV). In addition, the improvement of activity of ETS-10 by Ag ion exchange may be also due to the reduction of Ag ions to metallic Ag during photocatalysis by the photogenerated conduction band electrons, which thus enhances the electron–hole separation and reduces recombination [29]. It is possible that both Co isomorphous substitution and Ag ion exchange/subsequent Ag ion reduction may have affected the outer surface of ETS-10 at the level beyond that probed here with FE-SEM (i.e., photocatalytically active sites accessible on the external surface and/or at defects sites where the pore sizes have become enlarged). Since MB is most likely photodegraded on the outer ETS-10 surfaces, it is therefore difficult to unambiguously compare the performance of the unmodified ETS-10 and both modified (i.e., Co-ETS-10, and Ag^+-ETS-10) materials. Currently, a systematic investigation of transition metal isomorphous substitution and silver ion exchange is conducted to improve the photocatalytic activity of ETS-10. In addition, more effort is being made to better understand the mechanism of photocatalysis on these modified ETS-10 samples.

4. Conclusions

Light distribution analysis for a single ETS-10-coated quartz optical fiber showed a similar attenuation coefficient α for three different film thicknesses; however, lower extinction coefficients ε were determined for the thicker films compared to the thinnest film prepared. The nearly constant α values suggested a similar optical fiber surface coverage with ETS-10 crystals at the fiber/film interface for each film thickness. The decrease of ε values with increasing film thickness suggested less contact per unit film thickness between light and the crystals inside the thicker films, likely because ETS-10 crystals in the thicker multilayer ETS-10 films were

more loosely packed compared to crystals in the thinnest monolayer ETS-10 film.

Based on the light distribution analysis in a single ETS-10-coated optical fiber, an OFR system containing uniformly distributed ETS-10-coated fibers with film thickness of ~1.5 μm and coating length of 15 cm was fabricated. The results of photocatalytic degradation of MB conducted in this OFR system under UV light irradiation showed that ETS-10 activity increased upon increasing film thickness from ~0.5 to ~1.5 μm. This was consistent with the more extensive light absorption in the thicker ETS-10 films determined from the light propagation analysis in a single fiber. Although higher reaction rates were obtained at higher light intensities in the OFR system, the apparent quantum efficiency in photodegradation of MB decreased with increasing light intensity. This is consistent with the notion that the rate of electron–hole recombination increases relative to the interfacial charge transfer rate at high light intensity.

All ETS-10 samples investigated (i.e., as-synthesized, Ag ion-exchanged, and isomorphously substituted with Co) showed the apparent quantum efficiencies ~4–5 times higher in the OFR than in the slurry reactor. This improvement can be attributed to the unique light/photocatalyst/reactant contact in the OFR configuration, where the light transmitted out of optical fibers directly reaches the ETS-10 photocatalyst coated on the fiber surface without passing through the liquid, as is done in the slurry reactor. The high packing density of the optical fibers in the fabricated OFR system provided high illuminated ETS-10 surface area within a reactor volume, which also contributed to the improved performance.

Acknowledgements

The authors thank NASA for financial support. Zhaoxia Ji also acknowledges Robert Egan for assistance in building the optical fiber reactor.

References

[1] S.M. Kuznicki, Large-pored crystalline titanium molecular sieve zeolites, US Patent 4,853,202, 1989.
[2] J. Rocha, Z. Lin, Microporous mixed octahedral-pentahedral-tetrahedral framework silicates, Reviews in Mineralogy & Geochemistry 57 (2005) 173–201.
[3] M.W. Anderson, O. Terasaki, T. Ohsuna, A. Philippou, S.P. MacKay, A. Ferreira, J. Rocha, S. Lidin, Structure of the microporous titanosilicate ETS-10, Nature 367 (1994) 347–351.
[4] E. Borello, C. Lamberti, S. Bordiga, A. Zecchina, C.O. Arean, Quantum-size effects in the titanosilicate molecular sieve, Applied Physics Letters 71 (1997) 2319–2321.
[5] F.X. Llabrés i Xamena, P. Calza, C. Lamberti, C. Prestipino, A. Damin, S. Bordiga, E. Pelizzetti, A. Zecchina, Enhancement of the ETS-10 titanosilicate activity in the shape-selective photocatalytic degradation of large aromatic molecules by controlled defect production, Journal of the American Chemical Society 125 (2003) 2264–2271.
[6] S. Uma, S. Rodrigues, I.N. Martyanov, K.J. Klabunde, Exploration of photocatalytic activities of titanosilicate ETS-10 and transition metal incorporated ETS-10, Microporous and Mesoporous Materials 67 (2004) 181–187.
[7] M.J. Nash, S. Rykov, R.F. Lobo, D.J. Doren, I. Wachs, Photocatalytic activity of vanadium-substituted ETS-10, Journal of Physical Chemistry C 111 (2007) 7029–7037.
[8] Y. Shiraishi, D. Tsukamoto, T. Hirai, Selective photocatalytic transformations on microporous titanosilicate ETS-10 driven by size and polarity of molecules, Langmuir 24 (2008) 12658–12663.
[9] G. Guan, T. Kida, K. Kusakabe, K. Kimura, E. Abe, A. Yoshida, Photocatalytic activity of CdS nanoparticles incorporated in titanium silicate molecular sieves of ETS-4 and ETS-10, Applied Catalysis A: General 295 (2005) 71–78.
[10] P. Atienzar, S. Valencia, A. Corma, H. García, Titanium-containing zeolites and microporous molecular sieves as photovoltaic solar cells, ChemPhysChem 8 (2007) 1115–1119.
[11] H.D. Lasa, B. Serrano, M. Salaices, Photocatalytic Reaction Engineering, Springer, New York, 2005.
[12] K. Hofstadler, R. Bauer, S. Novalic, G. Heisler, New reactor design for photocatalytic wastewater treatment with TiO_2 immobilized on fused-silica glass fibers: photomineralization of 4-chlorophenol, Environmental Science & Technology 28 (1994) 670–674.
[13] N.J. Peill, M.R. Hoffmann, Development and optimization of a TiO_2-coated fiber-optic cable reactor: photocatalytic degradation of 4-chlorophenol, Environmental Science & Technology 29 (1995) 2974–2981.
[14] N.J. Peill, M.R. Hoffmann, Chemical and physical characterization of a TiO_2-coated fiber optic cable reactor, Environmental Science & Technology 30 (1996) 2806–2812.
[15] W. Choi, J.Y. Ko, H. Park, J.S. Chung, Investigation on TiO_2-coated optical fibers for gas-phase photocatalytic oxidation of acetone, Applied Catalysis B: Environmental 31 (2001) 209–220.
[16] R.-D. Sun, A. Nakajima, L. Watanabe, T. Watanabe, K. Hashimoto, TiO_2-coated optical fiber bundles used as a photocatalytic filter for decomposition of gaseous organic compounds, Journal of Photochemistry and Photobiology A: Chemistry 136 (2000) 111–116.
[17] W. Wang, Y. Ku, Photocatalytic degradation of gaseous benzene in air streams by using an optical fiber photoreactor, Journal of Photochemistry and Photobiology A: Chemistry 159 (2003) 47–59.
[18] J.C.S. Wu, H.-M. Lin, C.-L. Lai, Photo reduction of CO_2 to methanol using optical-fiber photoreactor, Applied Catalysis A: General 296 (2005) 194–200.
[19] H. Lin, K.T. Valsaraj, Development of an optical fiber monolith reactor for photocatalytic wastewater treatment, Journal of Applied Electrochemistry 35 (2005) 699–708.
[20] D.R. Lide (Ed.), CRC Handbook of Chemistry and Physics, CRC Press, Boca Raton, FL, 1995.
[21] J. Rocha, A. Ferreira, Z. Lin, M.W. Anderson, Synthesis of microporous titanosilicate ETS-10 from $TiCl_3$ and TiO_2: comprehensive study, Microporous and Mesoporous Materials 23 (1998) 253–263.
[22] T. Zhang, T. Oyama, A. Aoshima, H. Hidaka, J. Zhao, N. Serpone, Photooxidative N-demethylation of methylene blue in aqueous TiO_2 dispersions under UV irradiation, Journal of Photochemistry and Photobiology A: Chemistry 140 (2001) 163–172.
[23] A. Eldewik, R.F. Howe, Cobalt substitution in ETS-10, Microporous and Mesoporous Materials 48 (2001) 65–71.
[24] I. Tiscornia, S. Irusta, P. Prádanos, C. Téllez, J. Coronas, J. Santamaria, Preparation and characterization of titanosilicate Ag-ETS-10 for propylene and propane adsorption, Journal of Physical Chemistry C 111 (2007) 4702–4709.
[25] Y. Goa, P. Wu, T. Tatsumi, Liquid-phase knowledge reactions over modified basic microporous titanosilicate ETS-10, Journal of Catalysis 224 (2004) 107–114.
[26] H.F. Lin, Photocatalysis in a novel semiconducting optical fiber monolithic reactor for wastewater treatment, Ph.D. dissertation, 2005.
[27] X. Yan, T. Ohno, K. Nishijima, R. Abe, B. Ohtani, Is methylene blue an appropriate substrate for a photocatalytic activity test? A study with visible-light responsive titania, Chemical Physics Letters 429 (2006) 606–610.
[28] N.J. Peill, M.R. Hoffmann, Mathematical model of a photocatalytic fiber-optic cable reactor for heterogeneous photocatalysis, Environmental Science & Technology 32 (1998) 398–404.
[29] V. Vamathevan, H. Tse, R. Amal, G. Low, S. McEvoy, Effects of Fe^{3+} and Ag^{+} ions on the photocatalytic degradation of sucrose in water, Catalysis Today 68 (2001) 201–208.